PERIÓDICO TCHÊ QUÍMICA
ARTIGO ORIGINAL

MÉTODOS PARA ENDURECIMENTO E MELHORIA DAS CARACTERÍSTICAS DE FADIGA DE AMOSTRAS DE LIGAS DE NÍQUEL CROMO-FERRO E TITÂNIO

METHODS FOR HARDENING AND IMPROVEMENT OF FATIGUE CHARACTERISTICS OF TITANIUM AND IRON-CHROMIUM NICKEL ALLOY SAMPLES

МЕТОДЫ ПОВЫШЕНИЯ ПРОЧНОСТИ И УСТАЛОСТНЫХ ХАРАКТЕРИСТИК ОБРАЗЦОВ, ИЗГОТОВЛЕННЫХ ИЗ СПЛАВОВ ТИТАНА И ЖЕЛЕЗОХРОМОНИКЕЛЕВЫХ СПЛАВОВ

SKVORTSOV, Arkadiy A.[1]*; GNATYUK, Evgeniya O.[2]; RYBAKOVA, Margarita R.[3]; BURUKIN, Ivan V.[4];

[1,3,4] Moscow Polytechnic University; Department of Dynamics, Strength of Machines and Resistance of Materials; Moscow – Russian Federation

[2] JC “United Engine Corporation”; Department of Materials Science; Moscow – Russian Federation

** Corresponding author*
e-mail: SkvortsovAA2009@yandex.ru

Received 13 November 2019; received in revised form 29 April 2020; accepted 05 June 2020

RESUMO

Este trabalho descreve o procedimento para determinar tensões residuais na superfície usando o método mecânico e quatro métodos de endurecimento de amostras. A urgência do problema declarado no artigo se deve ao fato de que as tensões de tração superficial que surgem na fabricação de peças altamente carregadas podem reduzir significativamente as características mecânicas, de recursos e de fadiga dos produtos. O objetivo do estudo foi endurecer amostras de ligas de titânio e ferro-cromo-níquel para melhorar suas características de resistência, fadiga, recursos e determinar tensões residuais por remoção camada por camada das camadas estudadas por ataque eletroquímico. A determinação das tensões residuais da superfície foi realizada mecanicamente, utilizando um complexo de medição e cálculo durante a gravação contínua do metal a partir da superfície de teste da amostra, o que possibilitou medir as tensões residuais em diferentes profundidades e determinar a energia do estado de estresse da superfície. As tensões residuais foram calculadas a partir da deformação da parte restante da amostra com uma mudança na profundidade das camadas estudadas. O endurecimento das amostras foi realizado de quatro maneiras, a saber: endurecimento por ultrassom; cura por ultrassom + Rosler (processamento de vibração); Rosler (processamento de vibração) + cura por ultrassom; Rosler (processamento de vibração) + endurecimento por ultrassom. Os resultados do estudo mostraram que a superfície dos produtos é uma área mais fraca que a interna. Após a têmpera, surgem tensões compressivas na superfície de todas as amostras de ligas de titânio e ferro-cromo-níquel. O caso preferido de endurecimento é o segundo (endurecimento ultrassônico + endurecimento centrífugo). A presença de tensões compressivas residuais nas camadas externas dos produtos aumenta seu limite de fadiga em ± 20%. Os resultados do trabalho podem ser usados para fabricar produtos com altas características mecânicas, de recursos e de fadiga.

Palavras-chave: *tensões residuais, ultrassom, deformação, resistência, macro estresses.*

ABSTRACT

This work describes the procedure for determining residual surface stresses using the mechanical method and four methods of hardening samples. The urgency of the problem stated in the article is due to the fact that surface tensile stresses arising in the manufacture of highly loaded parts can significantly reduce the mechanical, resource and fatigue characteristics of products. The aim of the study was to harden samples of titanium and iron-chromium-nickel alloys to improve their strength, fatigue and resource characteristics and determine residual stresses by layer-by-layer removal of the studied layers by electrochemical etching. The determination of surface residual stresses was carried out mechanically using a measuring and calculation complex during continuous etching of the metal from the test surface of the sample, which made it possible to measure the residual stresses at different depths and determine the energy of the surface stress state. Residual stresses were calculated from the deformation of the remaining part of the sample with a change in the depth of the studied layers. The hardening of the samples was carried out in four ways, namely: ultrasonic hardening; ultrasonic curing + Rosler (vibration

DOI: 10.52571/PTQ.v17.n35.2020.37_SKVORTSOV_pgs_425_436.pdf

processing); Rosler (vibration processing) + ultrasonic curing; Rosler (vibration processing) + ultrasonic hardening. The results of the study showed that the surface of the products is a weaker area than the inside. After quenching, surface compressive stresses arise for all samples of titanium and iron-chromium-nickel alloys. The preferred case of hardening is the second (ultrasonic hardening + centrifugal hardening). The presence of residual compressive stresses in the outer layers of the products increases their fatigue limit by ≈20%. The results of the work can be used to manufacture products with high mechanical, resource and fatigue characteristics.

Keywords: *residual stresses, ultrasound, deformation, strength, macrostresses.*

АННОТАЦИЯ

В данной работе описана процедура определения остаточных поверхностных напряжений с использованием механического метода и четырех способов упрочнения образцов. Актуальность заявленной в статье проблемы обусловлена тем, что поверхностные растягивающие напряжения, возникающие при изготовлении высоконагруженных деталей, могут существенно снизить механические, ресурсные и усталостные характеристики изделий. Целью исследования является закалка образцов из титановых и железо-хромоникелевых сплавов для улучшения их прочностных, усталостных и ресурсных характеристик и определения остаточных напряжений путем послойного снятия исследуемых слоев методом электрохимического травления. Определение поверхностных остаточных напряжений проводилось механическим методом с использованием измерительно-расчетного комплекса при непрерывном травлении металла с исследуемой поверхности образца, что позволило измерить остаточные напряжения на разных глубинах залегания и определить энергию напряженного состояния поверхности. Остаточные напряжения рассчитывались по деформации оставшейся части образца с изменением глубины залегания исследуемых слоев. Упрочнение образцов было проведено четырьмя способами, а именно: ультразвуковое упрочнение; ультразвуковое отверждение + рослер (виброобработка); Рослер (виброобработка) + ультразвуковое отверждение; Рослер (виброобработка) + ультразвуковое упрочнение. Результаты исследования показали, что поверхность изделий является более слабой областью, чем внутренняя часть. После закалки возникают поверхностные сжимающие напряжения для всех образцов из титана и железо-хромоникелевых сплавов. Предпочтительным случаем упрочнения является второй (ультразвуковое упрочнение + центробежное упрочнение). Наличие остаточных сжимающих напряжений во внешних слоях изделий увеличивает предел их усталости на ≈20%. Результаты работы могут быть использованы для изготовления изделий с высокими механическими, ресурсными и усталостными характеристиками.

Ключевые слова: *остаточные напряжения, ультразвук, деформация, прочность, макронапряжения.*

1. INTRODUCTION:

When producing high-loaded details, one of the problems is the presence of surface tensile stresses (Gnyusov *et al*., 2017; Hou *et al*., 2018). They can substantially reduce the mechanical, resource, and fatigue characteristics of products (Wojtaszek *et al*., 2016; Sakhvadze *et al*., 2017; Pei & Duan, 2017; Huang *et al*., 2018). The residual stresses exist in products in the absence of external actions. Three types of stresses are distinguished: macro stresses, micro stresses, and elastic stresses (Birger, 1963; Colegrove *et al*., 2013; Hamad & Hassan, 2018; Astapov *et al*., 2019a; Astapov *et al*., 2019b; Cui *et al*., 2020; Su *et al*., 2020).

The main methods to determine residual stresses are mechanical and x-ray methods (Liu *et al.,* 2019; Sunder, 2016; Mohanty & Muduli, 2020). The mechanical process is most widely spread because it uses the same concepts of stresses and deformations of elastic body mechanics as those used when calculating the strength, rigidity, and stability of details. The mechanical method of determination of residual stresses is based on cutting a sample from detail and subsequent layer-by-layer removal of the layers under investigation using electrochemical etching (Antolovich & Armstrong, 2014; Mustafin, 2006; Samarin *et al*., 2019; Makarenko & Kuznetsova, 2019; Ding *et al*., 2015).

The object of the work was to harden samples made of titanium and iron-chromium-nickel alloys for improvement of their strength, fatigue, and resource characteristics and determination of residual stresses by layer-by-layer removal of the studied layers using electrochemical etching.

2. MATERIALS AND METHODS:

The determination of residual surface stresses was made by the mechanical method using a measuring-calculating complex at the continuous etching of metal from the sample surface under investigation (Figure 1). Such a

plant measures residual stresses at different occurrence depths and determines the energy of surface stressed state, as well as makes it possible to optimize and control the stability of technological processes (Figure 2).

An experiment began by cutting a sample of standard sizes 50×4×2 mm (Figure 3). Then the sample was fastened into a holder (investigated face down); the holder and surface that was not subjected to etching were coated with paraffin. A steel ball was fastened in paraffin at the sample upper surface where deformation was measured (for contact with an inductive transducer). Then the holder with the sample was suspended to a carriage of the gage post, and the steel ball was brought to the inductive transducer to the point of maximal contacting. After this, the carriage was put into the electrolyte, and the etching process began. The balance became disturbed, causing the sample to deform. The residual stresses σ were calculated from the deformation of the remaining part of the sample, with changing occurrence depth of the layers studied (Birger, 1963; Gnatyuk, 2017; Lu *et al*., 2018; Madzivhandila *et al*., 2019).

3. RESULTS AND DISCUSSION:

3.1. Determination of residual stresses

Let us consider the determination of axial residual stresses in a prismatic rod. We assume that, except for small areas at the ends of the rod, the residual stresses are constant along its length. To determine the residual stresses, we will sequentially remove the ABCD layers of materials (Figure 4) located in the zone of constant (along the length) stresses. The end sections are not removed; they are placed in the grips of the device.

The residual stresses σ in the surface layers of the initial detail were determined as a sum of stresses relaxed because of sample cutting from the detail (σ_d) and a nonlinear component ($\sigma_{n.l.}$) due to removal of layers from the sample surface (Equation 1). Depending on the sample thickness and value of mechanical stresses in the layers under investigation, layers separation from the detail may lead to its bending F_b and (or) change of its length ε_b. In this case, the variation of the initial stresses may be calculated as a linear component from their occurrence depth (Equation 2). Here E is the material modulus of elasticity; F_b is the bending because of sample cutting from the detail; K_0 and K_1 are the coefficients representing both form and sizes of the sample; K_{amp} is the deformation amplification coefficient at different ways of fastening the sample and transducer in the process of cutting; ε_b is sample's relative extension at cutting.

Let us determine the residual stresses $\sigma_{n.l.}$ acting in the rod at a distance a from the upper face of the rod (Figure 4). As a result of the removal of a layer of material with a thickness a, the remaining part of the rod is deformed under the action of stresses along the planes AB and DC.

Let stresses $\sigma_{n.l.}(a)$ act at a distance ξ from the upper face. The bending moment M from stresses on the face AB relative to the middle of the rod height (point O) is (Equation 3), where b is the width of the rod. If the rod is bent by the concentrated moments M at the end, then the deflection is (Equation 4), where l, h is the length and thickness of the rod, respectively, J is the moment of inertia of the cross-section (Equation 5). Neglecting the influence of axial forces on bending and taking into account (Equation 4) and (Equation 5), we find (Equation 6). Transferring the value $(h-a)^3$ to the left side of the equality and differentiating the integral over the upper limit a, we obtain (Equation 7). From (Equation 7) at $a = 0$ we obtain the formula for determining the residual stresses in the outer layer (Equation 8). After differentiating equality (Equation 7) with respect to a, we have (Equation 9). Integrating both sides of this equality, we obtain (Equation 10).

Given the relation (Equation 8), we can obtain the equation (Equation 11). The residual stresses varying with occurrence depth of the removing layers were calculated from the expression that takes into account not only the measured deformation for each current depth but also those residual deformations that relaxed due to the removal of the previous layers. The residual stresses component that varies with etching depth was calculated for prismatic samples in real time scale (Equation 11). Here L_{et} is the etched layer length; H is the sample thickness; F is the current value of sample deformation; $\frac{dF}{da}$ is deformation variation with occurrence depth of the layers under investigation; a_i is the current depth of removed layers; ξ is the total current deformation.

When determining the residual stresses, the balance of forces over the sample thickness is violated because of etching of the layers studied that are in the stress state, and the sample bends. The stresses in the layer under investigation are calculated from that bending (deformation). In this

case, the balance of forces is restored, and partial relaxation of stress state occurs on the opposite side of the sample, in accordance with the bending moment (Sangid, 2013; Ahmad *et al.,* 2018; Aguilera-Correa *et al*., 2019). Due to the specially chosen etching conditions, an exact calculation of the depth of etched layers is done from the amount of passed electric current according to Faraday's law (Equation 12).

Here *a* is the etched layer depth; *t* is the etching time; *I* is current in the etching series; *α* is the effective electrochemical equivalent; *ρ* is the sample material density; *B* is the sample width. Shown in Figures 5 and 6 are the samples of titanium and iron-chromium-nickel alloys after etching. Figures 7 and 8 present the diagrams of surface residual stresses distribution in the samples of titanium (Li *et al.,* 2016; Kumar *et al*., 2017; Kim *et al.,* 2013) and iron-chromium-nickel alloys (Jiang & Zhao, 2012; Debroy *et al.,* 2018). One can see that surface tensile stresses are present on samples of both types. The presence of such stresses (from 50 MPa and more) considerably reduces vibration and fatigue strength of the product (Malaki & Ding, 2015; Zhu *et al.,* 2017; Lin *et al*., 2018; Wang *et al*., 2020).

To solve the above problem, hardening of samples was performed in four ways: 1 – ultrasonic hardening; 2 – ultrasonic hardening + Rosler (vibratory finishing); 3 – Rosler (vibratory finishing) + ultrasonic hardening; 4 – Rosler (vibratory finishing) + ultrasonic hardening (He *et al*., 2018; Sangid, 2013). In all four cases, the parameters of ultrasonic hardening remained unchanged: amplitude of 100 μm and rated frequency of 20 kHz.

3.2. Centrifugal Hardening (Rosler)

Centrifugal treatment (Figure 9) is a high-performance method for finishing and hardening parts. The method of volumetric centrifugal treatment consists in the fact that the granular processing medium with the details is rotationally driven around the vertical axis so that it takes on the shape of a torus in which particles move along spiral paths. The machined parts are loaded into the working chamber and moved together with the working environment. Hardening is carried out due to the relative movement and interaction of the granular medium and the parts wetted by a liquid continuously supplied to the working chamber.

3.3. Ultrasonic hardening

The strain hardening of the surface layer of samples during ultrasonic hardening (Figure 10) is carried out due to the kinetic energy of steel balls randomly moving in a spatially limited volume. The surface treatment takes place in the “cloud” of the working medium (balls) simultaneously from two sides. This type of treatment causes an increase in hardness of the surface layer by 18% and an increase in surface compressive stresses to 1000 MPa. The depth of the riveted layer is 20-25 μm. Structural changes in the surface zones of the part cause an increase in the durability of products up to 1.5 times at cyclic stresses of 1650-2600 MPa. After hardening of samples in four ways, residual surface stresses were measured, and the diagrams of their distribution were obtained (Furuya, 2013; Kim *et al*., 2016; Cai *et al*., 2017; Zhan *et al.,* 2018; Su *et al.,* 2018; Klimenko *et al*., 2018; Qiao *et al*., 2019; Zhang *et al*., 2020). The results of the measurements are presented in Figures11 and 12.

One can see from figures that after hardening, there are surface compressive stresses for all samples made of titanium and iron-chromium-nickel alloys. The preferred case of hardening is the second (ultrasonic hardening + centrifugal hardening). In this case, the maximum compressive residual stresses reach 550 MPa at a depth of 50 μm. The presence of residual compressive stresses in the outer layers of products increases their fatigue limit by ≈20%.

4. CONCLUSIONS:

The results of the investigations showed that the surface of products studied is a “weaker” area than the interior. Therefore, any process that leads to appearance and increase of surface compressive stresses will be positive for material operation. After quenching, surface compressive stresses arise for all samples of titanium and iron-chromium-nickel alloys. The preferred case of hardening is the second (ultrasonic hardening + centrifugal hardening). The presence of residual compressive stresses in the outer layers of the products increases their fatigue limit by ≈20%. The results of the work can be used to manufacture products with high mechanical, resource and fatigue characteristics.

5. ACKNOWLEDGMENTS:

This study is conducted with financial support from the Ministry of Education and Science of the Russian Federation (project No. FZRR-2020-0023/code 0699-2020-0023).

6. REFERENCES:

1. Aguilera-Correa, J.-J., Auñón, Á., Boiza-Sánchez, M., Mahillo-Fernández, I., Mediero, A., Eguibar-Blázquez, D., Conde, A., Arenas, M.-Á., de-Damborenea, J.-J., Cordero-Ampuero, J., & Esteban, J. (2019). Urine aluminum concentration as a possible implant biomarker of pseudomonas aeruginosa infection using a fluorine- and phosphorus-doped Ti-6Al-4V alloy with osseointegration capacity. *ACS Omega*, *4*(7), 11815-11823
2. Ahmad, B., van der Veen, S. O., Fitzpatrick, M. E., & Guo, H. (2018). Measurement and modelling of residual stress in wire-feed additively manufactured titanium. *Materials Science and Technology*, *34*(18), 2250-2259. https://doi.org/10.1080/02670836.2018.1528747
3. Antolovich, S. D., & Armstrong, R. W. (2014). Plastic strain localization in metals: Origins and consequences. *Progress in Materials Science*, *59*(1), 1-160. https://doi.org/10.1016/j.pmatsci.2013.06.001
4. Astapov, A.N., Kuznetsova, E.L., & Rabinskiy, L.N. (2019b). Operating capacity of anti-oxidizing coating in hypersonic flows of air plasma. *Surface Review and Letters, 26*(2), Article number 1850145.
5. Astapov, A.N., Lifanov, I.P., & Rabinskiy, L.N. (2019a). Perspective heat-resistant coating for protection of C_f/SiC composites in air plasma hypersonic flow. *High Temperature, 57*(5), 744-752.
6. Birger, I. A. (1963). *Residual stresses*. Moscow: Russian Federation: Mashgiz.
7. Cai, Z.B., Pang, X.J., Cui, X.F., Wen, X., Liu, Z., Dong, M.L., Li, Y., & Jin, G. (2017). In situ laser synthesis of high entropy alloy coating on Ti-6Al-4V alloy: Characterization of microstructure and properties. *Materials Science Forum*, *898*, 643–650. https://doi.org/10.4028/www.scientific.net/msf.898.643
8. Colegrove, P. A., Coules, H. E., Fairman, J., & Martina, F. (2013). Microstructure and residual stress improvement in wire and arc additively manufactured parts through high-pressure rolling. *Journal of Materials Processing Technology*, *213*(10), 1782-1791. https://doi.org/10.1016/j.jmatprotec.2013.04.012
9. Cui, F., Wang, G., Yu, D., Gan, X., Tian, Q., & Guo, X. (2020). Towards “zero waste” extraction of nickel from scrap nickel-based superalloy using magnesium. *Journal of Cleaner Production*, *262*, article number 121275.
10. Debroy, T., Wei, H. L., Zuback, J. S., Elmer, J. W., Beese, A. M., & Zhang, W. (2018). Additive manufacturing of metallic components – Process, structure and properties. *Progress in Materials Science*, *92*, 112-224. https://doi.org/10.1016/j.pmatsci.2017.10.001
11. Ding, D., Pan, Z., Cuiuri, D., & Li, H. (2015). Wire-feed additive manufacturing of metal components: technologies, developments and future interests. *International Journal of Advanced Manufacturing Technology*, *81*(1-4), 465-481. https://doi.org/10.1007/s00170-015-7077-3
12. Furuya, Y. (2013). Visualization of internal small fatigue crack growth. *Materials Letters*, *112*, 139-141. https://doi.org/10.1016/j.matlet.2013.09.015
13. Gnatyuk, E.O. (2017). Statement of the experiment for the limiting state of samples from materials VT8 and IP718VD under biharmonic loading. In *Proceedings of the MIKMUS* (pp. 465-467). Moscow, Russian Federation: MIKMUS.
14. Gnyusov, S.F., Rotshtein, V.P., Mayer, A.E., Astafurova, E.G., Rostov, V.V., Gunin, A.V., & Maier, G.G. (2017). Comparative study of shock-wave hardening and substructure evolution of 304L and Hadfield steels irradiated with a nanosecond relativistic high-current electron beam. *Journal of Alloys and Compounds*, *714*, 232–244.
15. Hamad, D., & Hassan, B. (2018). Evaluation of salivary nickel, chromium and iron ions in patients treated with fixed orthodontic appliances in vivo study. *Erbil Dental Journal (EDJ)*, *1*(2), 109-116. https://doi.org/10.15218/edj.2018.15
16. He, Y., Xiao, G., Li, W., & Huang, Y. (2018). Residual stress of a titanium alloy after belt grinding and its impact on the fatigue life. *Materials*, *11*(11), article number 2218. https://doi.org/10.3390/ma11112218

17. Hou, X., Liu, Z., Wang, B., Lv, W., Liang, X., & Hua, Y. (2018). Stress-strain curves and modified material constitutive model for Ti-6Al-4V over the wide ranges of strain rate and temperature. *Materials*, *11*, article number 938.

18. Huang, S., Zhu, Y., Guo, W., Peng, P., & Diao, X. (2018). Effects of laser shock processing on impact toughness of Ti-17 titanium alloy. *High Temperature Materials and Processes*, *37*(4), 325-332. doi: https://doi.org/10.1515/htmp-2016-0106

19. Jiang, J., & Zhao, M. (2012). Influence of residual stress on stress concentration factor for high strength steel welded joints. *Journal of Constructional Steel Research*, *72*, 20-28. https://doi.org/10.1016/j.jcsr.2011.09.007

20. Kim, J.-C., Cheong, S.-K., & Noguchi, H. (2013). Residual stress relaxation and low- and high- cycle fatigue behavior of shot-peened medium – carbon steel. *International Journal of Fatigue*, *56*, 114-122. https://doi.org/10.1016/j.ijfatigue.2013.07.001

21. Kim, M.J., Yadav, P., & Lee, D.B. (2016). Isothermal and cyclic oxidation of Ti-6Al-4V alloy. *Defect and Diffusion Forum*, *369*, 99–103. https://doi.org/10.4028/www.scientific.net/ddf.369.99

22. Klimenko, D., Ozerov, M., Suresh, S., Stepanov, N., Tikhonovsky, M.A., Salishchev, G., & Zherebtsov, S. (2018). Microstructure Evolution and Properties of Ti-6Al-4V Alloy Doped with Fe and Mo during Deformation at 800°C. *Defect and Diffusion Forum*, *385*, 144-149.

23. Kumar, S., Chattopadhyay, K., & Singh, V. (2017). Effect of ultrasonic shot peening on LCF behavior of the Ti-6Al-4V alloy. *Journal of Alloys and Compounds*, *724*, 187-197. https://doi.org/10.1016/j.jallcom.2017.07.014

24. Li, P., Warner, D. H., Fatemi, A., & Phan, N. (2016). Critical assessment of the fatigue performance of additively manufactured Ti-6AL-4V and perspective for future research. *International Journal of Fatigue*, *85*, 130-143. https://doi.org/10.1016/j.ijfatigue.2015.12.003

25. Lin, D.G., Park, J.M., Kang, T.G., Chung, S.T., Kwon, Y.S., & Park, S.J. (2018). Powder injection molding of Ti-6Al-4V alloy for defect-free high performance titanium parts with low carbon/oxygen contents. *Key Engineering Materials*, *770*, 189–194. https://doi.org/10.4028/www.scientific.net/kem.770.189

26. Liu, C., Liu, D., Zhang, X., Ma, A., Ao, N., & Xu, X. (2019). Improving fatigue performance of Ti-6Al-4V alloy via ultrasonic surface rolling process. *Journal of Materials Science and technology*, *35*(8), 1555-1562. https://doi.org/10.1016/j.jmst.2019.03.036

27. Lu, J., Yang, Z., Li, Y., Huang, J., Zhao, X., & Yuan, Y. (2018). Effect of alloying chemistry on fireside corrosion behavior of Ni–Fe-based superalloy for ultra-supercritical boiler applications. *Oxidation of Metals*, *89*, 609–621. https://doi.org/10.1007/s11085-017-9804-7

28. Madzivhandila, T., Bhero, S., & Varachia, F. (2019). The influence of titanium addition on wettability of high-chromium white cast iron-matrix composites. *Journal of Composite Materials*, *53*(11), 1567–1576. https://doi.org/10.1177/0021998318804616

29. Makarenko, A.V., & Kuznetsova, E.L. (2019). Energy-efficient actuator for the control system of promising vehicles. *Russian Engineering Research, 39*(9), 776-779.

30. Malaki, M., & Ding, Y. (2015). A review of ultrasonic peening treatment. *Materials and Design*, *87*, 1072-1086. https://doi.org/10.1016/j.matdes.2015.08.102

31. Mohanty, J., & Muduli, R.C. (2020). Preparation of Fe–Ni Alloy Containing Low Cr and Ti from Red Mud Through Molten Salt Electrolysis. *Journal of The Institution of Engineers (India): Series C*, *101*, 401-406.

32. Mustafin, A. (2006). Two mutually loss-coupled lasers featuring astable multivibrator. *Physica D: Nonlinear Phenomena, 218*(2), 167-176.

33. Pei, Y., & Duan, Ch. (2017). Study on stress-wave propagation and residual stress distribution of Ti-17 titanium alloy by laser shock peening. *Journal of Applied Physics*, *122*, article number 193102.

34. Qiao, Y., Xu, D., Wang, S., Ma, Y., Chen, J., Wang, Y., & Zhou, H. (2019). Corrosion and tensile behaviors of Ti-4Al-2V-1Mo-1Fe and Ti-6Al-4V titanium alloys. *Metals, 9*, 1213.

35. Sakhvadze, G.Z., Pugachev, M.S. & Kikvidze, O.G. (2017). Two-sided laser shock processing. *Russian Engineering Research*, *37*, 40-45. https://doi.org/10.3103/S1068798X17010191

36. Samarin, I.V., Strogonov, A.Y., & Butuzov, S.Y. (2019). Evaluation model of integrated safety of fuel and energy complex facilities. *International Journal of Engineering and Advanced Technology, 8*(5), 2162-2167.

37. Sangid, M.D. (2013). The physics of fatigue crack initiation. *International Journal of Fatigue*, *57*, 58-72. https://doi.org/10.1016/j.ijfatigue.2012.10.009

38. Su, B., Wang, H., Cao, Y., Pei, X. & Hua, G. (2020). Local deformation and macro distortion of TC4 titanium alloy during laser shock processing. *The International Journal of Advanced Manufacturing Technology*, *106*, 5421-5428. https://doi.org/10.1007/s00170-020-05058-7

39. Su, B., Zhang, Y., Sun, G., & Ni, Z. (2018). Prediction of micro indention depth of titanium alloy during laser shock processing. *Japanese Journal of Applied Physics*, *57*(12), article number 122703. https://doi.org/10.7567/JJAP. 57.122703

40. Sunder, R. (2016). Why and how residual stress affects metal fatigue. *Springer Proceeding in Physics*, *175*, 489-504. https://doi.org/10.1007/978-3-319-26324-3_34

41. Wang, T., Qiao, W., Wang, Sh., Li, Zh., Wang, H. & Lei, J. (2020). Ti-6Al-4V alloy fabricated by laser direct deposition: Dynamic mechanical properties, constitutive model, and numerical simulation. *Surface Review and Letters*. Retrieved from https://www.worldscientific.com/doi/pdf/10.1142/S0218625X19501919

42. Wojtaszek, M., Sleboda, T., & Korpala, G. (2016). Hot processing of cast and PM Ti-6Al-4V alloy. *Archives of Metallurgy and Materials*, *61*(2B), 1115-1120.

43. Zhan, Y., Zhang, E., Ge, Y., & Liu, C. (2018). Residual stress in laser welding of titanium alloy based on ultrasonic laser technology. *Applied Sciences*, *8*(10), article number 1997. https://doi.org/10.3390/app8101997

44. Zhang, S.L., Yu, Y.C., Chen, W.Y., Qiu, M.K., & Liu, W L. (2020). Microstructure of Ti-based alloys after rapid solidification. *Materials Science Forum*, *993*, 313–320. https://doi.org/10.4028/www.scientific.net/msf.993.313

45. Zhu, S.-P., Yue, P., Yu, Z.-Y., & Wang, Q. (2017). A combined high and low cycle fatigue model for life prediction of turbine blades. *Materials*, *10*(7), article number 698. https://doi.org/10.3390/ma10070698

$$\sigma = \sigma_d + \sigma_{n.l.} \quad \text{(Eq. 1)}$$

$$\sigma_d = E\left\{\left(\frac{K_1}{K_{amp}}\right)\cdot F_b - K_0 \cdot \varepsilon_b\right\} \text{n} \quad \text{(Eq. 2)}$$

$$M = \int_0^a \sigma_{n.l.}(\xi)\left(\frac{1}{2}(h-a)-\xi\right)b d\xi \quad \text{(Eq. 3)}$$

$$f = \frac{Ml^2}{8EJ} \quad \text{(Eq. 4)}$$

$$J = \frac{b(h-a)^3}{12} \quad \text{(Eq. 5)}$$

$$F(a) = \frac{3l^2}{2E(h-a)^3}\cdot\int_0^a \sigma_{n.l.}(\xi)\left[\frac{1}{2}(h+a)-\xi\right]b d\xi \quad \text{(Eq. 6)}$$

$$(h-a)^2\frac{dF}{da}(a) - 3(h-a)^2 F(a) = \frac{3l^2}{2E}\left[\frac{1}{2}\int_0^a \sigma_{n.l.}(\xi)d\xi + \frac{1}{2}\sigma_{n.l.}(a)(h-a)\right] \quad \text{(Eq. 7)}$$

$$\sigma_{n.l.}(0) = \frac{4Eh^2}{3l^2}\frac{dF}{da}(0) \quad \text{(Eq. 8)}$$

$$(h-a)^2\frac{d^2F(a)}{da^2} - 6(h-a)\frac{dF(a)}{da} + 6F(a) = \frac{3l^2}{4E}\frac{d\sigma_{n.l.}(a)}{da} \quad \text{(Eq. 9)}$$

$$(h-a)^2\frac{dF(a)}{da} - 4(h-a)F(a) + 2\int_0^a F(\xi)d\xi - h^2\frac{dF(0)}{da} = \frac{3l^2}{4E}\left[\sigma_{n.l.}(a) - \sigma_{n.l.}(0)\right] \quad \text{(Eq. 10)}$$

$$\sigma_{n.l.} = \left(\frac{4E}{3L_{et}^2 K_{amp}}\right)\cdot\left[(H-a_i)^2\cdot\left(\frac{dF}{da}\right) - 4(H-a_i)F_{a_i} + 2\int_0^{a_i} F(\xi)d\xi\right] \quad \text{(Eq. 11)}$$

$$a = \frac{\alpha\cdot t\cdot\int_0^t I\text{dt}}{\rho\cdot L_{et}\cdot B} \quad \text{(Eq. 12)}$$

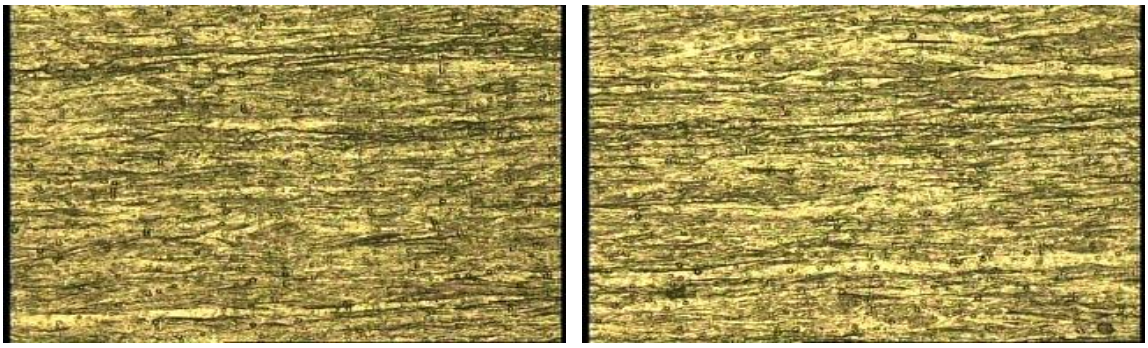

Figure 1. *Photo of the surface of titanium samples after machining* (*magnification* 100×)

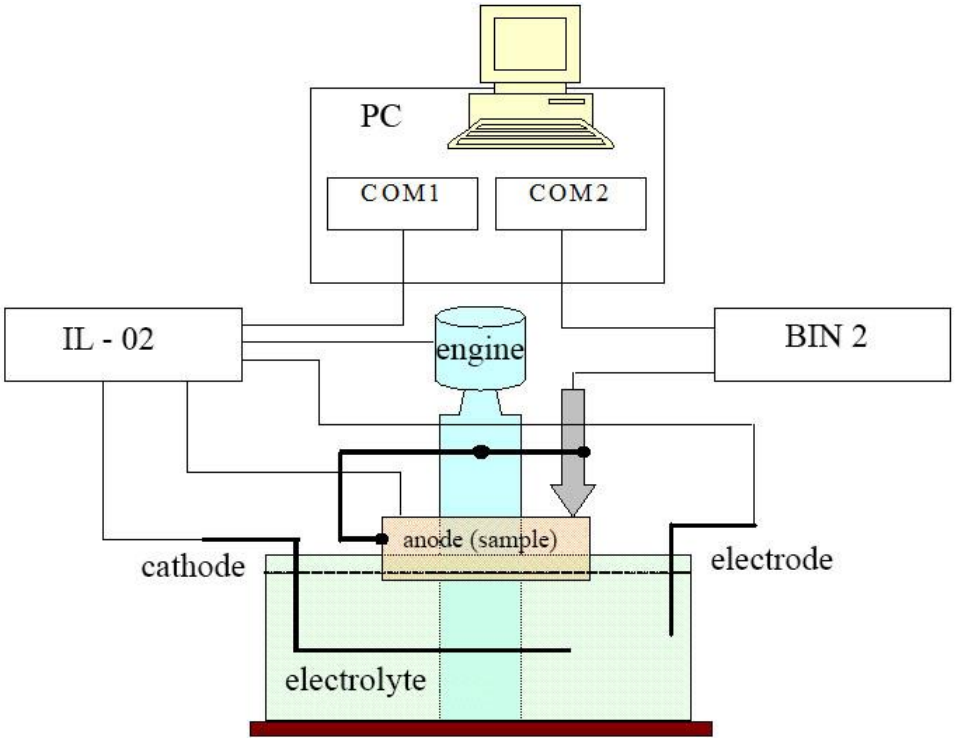

Figure 2. *Installation diagram: the electric current source IL-02 delivers electric current to a bath with electrolyte; BIN 2 measures sample deformation*

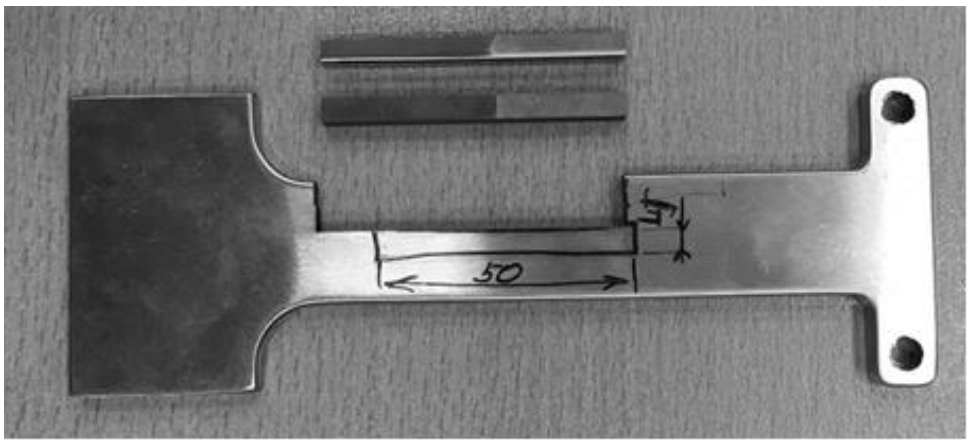

Figure 3. *The scheme of cutting samples for determining residual stresses*

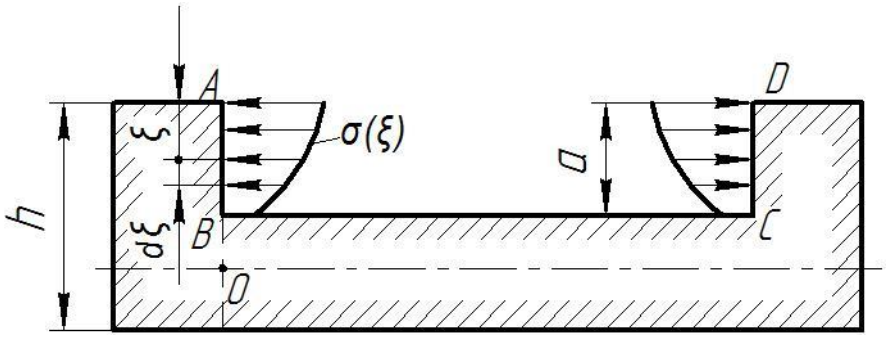

Figure 4. *The geometry of the rod when etching layers and emerging mechanical stresses*

Figure 5. *Sample of the titanium alloy after etching*

Figure 6. *Sample of the iron-chromium-nickel alloy after etching*

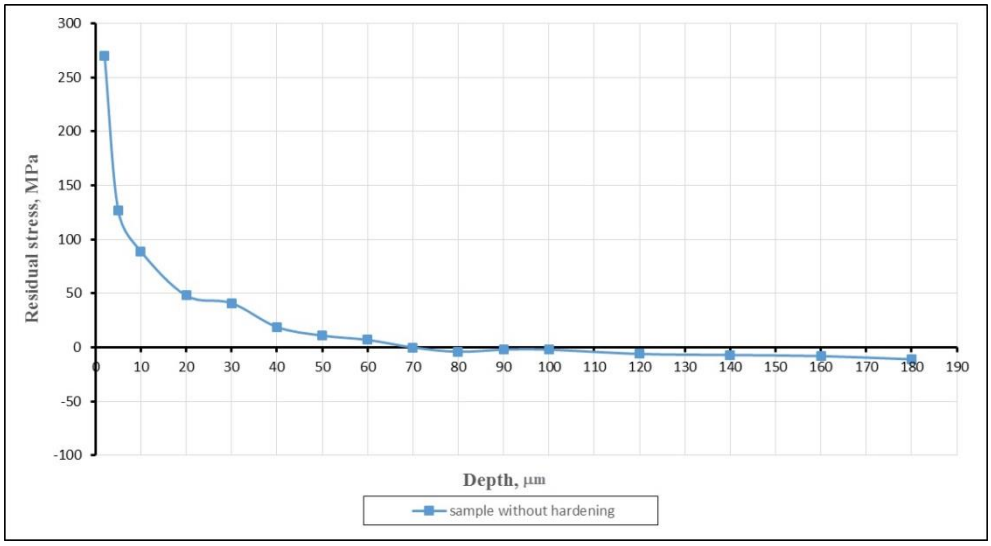

Figure 7. *Diagram of residual stresses distribution in a sample of titanium alloy before hardening*

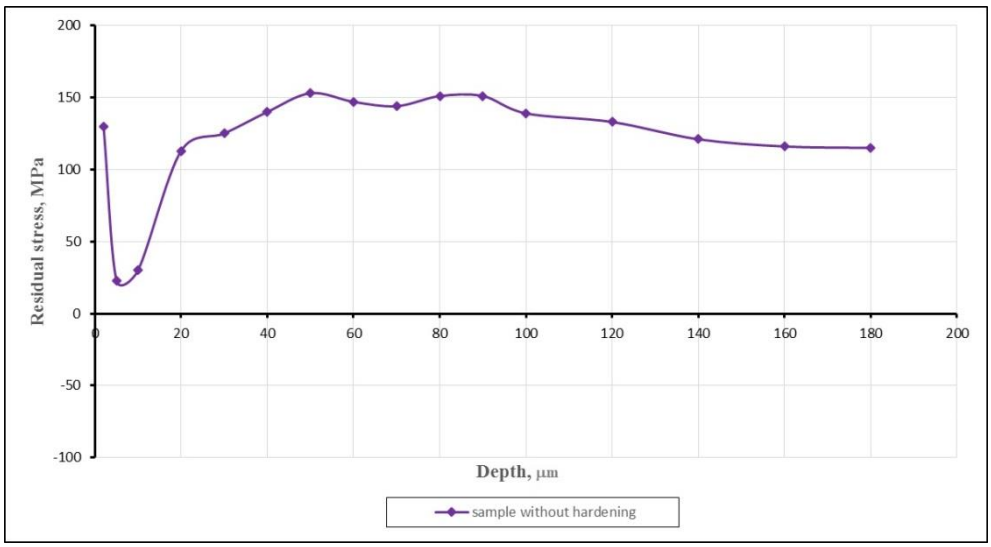

Figure 8. *Diagram of residual stresses distribution in a sample of iron-chromium-nickel alloy before hardening*

Figure 9. *Installation for centrifugal hardening treatment (Rosler)*

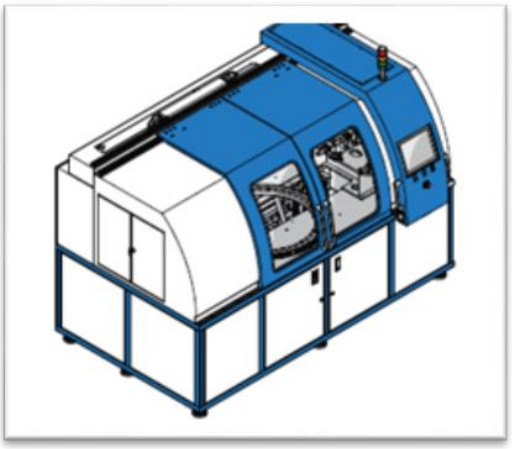

Figure 10. *Installation for ultrasonic hardening*

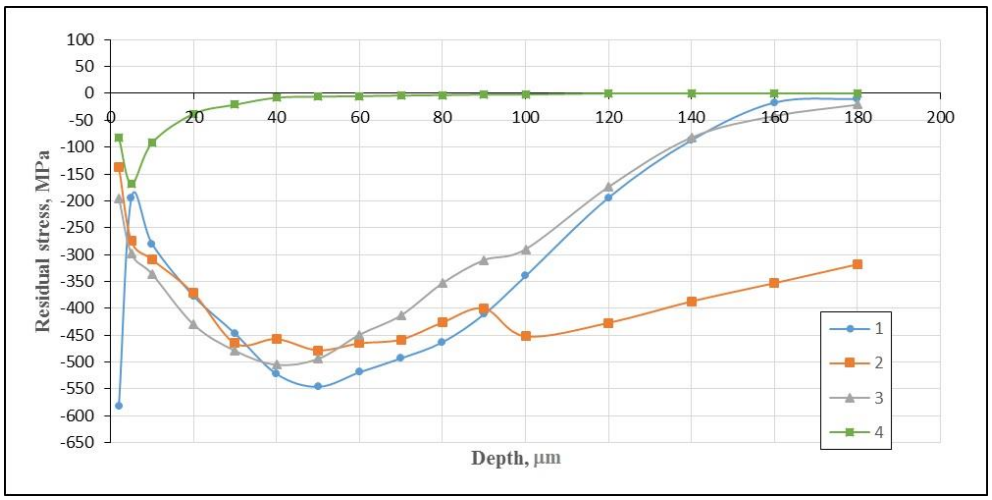

Figure 11. *Diagram of residual stresses distribution in samples of titanium alloy after hardening*

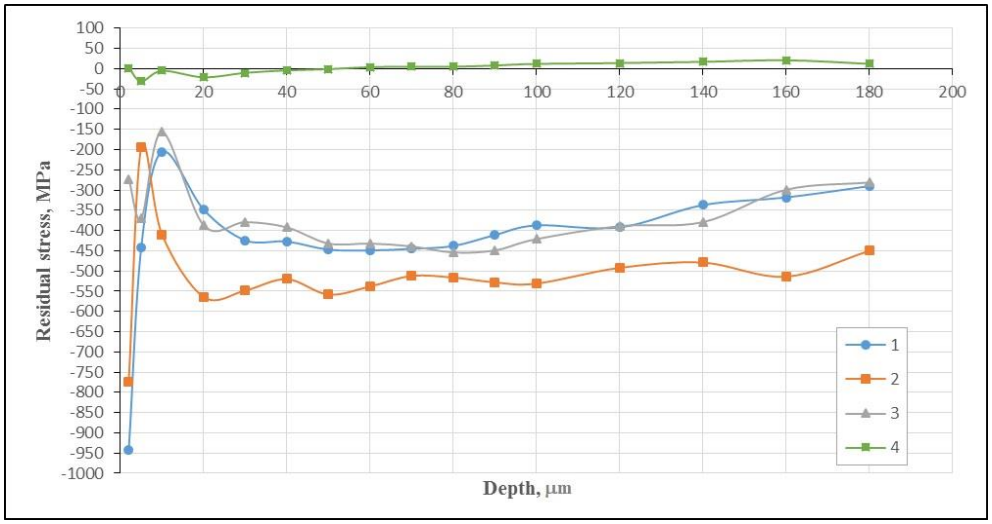

Figure 12. *Diagram of residual stresses distribution in samples of iron-chromium-nickel alloy after hardening*